Journal of Alloys and Compounds 946 (2023) 169484

Contents lists available at ScienceDirect

Journal of Alloys and Compounds

journal homepage: www.elsevier.com/locate/jalcom

Reversibility and thermal dependence of the martensitic transformation in a melt-spun $Ni_{55}Fe_{17}Ga_{26}Co_2$ Heusler alloy

A.F. Manchón-Gordón [a,*], A. Vidal-Crespo [b], J.S. Blázquez [b], M. Kowalczyk [c], J.J. Ipus [b], T. Kulik [c], C.F. Conde [b]

[a] Instituto de Ciencia de Materiales de Sevilla, ICMSE CSIC-Universidad de Sevilla, C. Américo Vespucio 49, Sevilla 41092, Spain
[b] Dpto. Física de la Materia Condensada, ICMSE-CSIC, Universidad de Sevilla, P.O. Box 1065, 41080 Sevilla, Spain
[c] Faculty of Materials Science and Engineering, Warsaw University of Technology, 141 Wołoska st., 02–507 Warsaw, Poland

ARTICLE INFO

Article history:
Received 21 December 2022
Received in revised form 24 February 2023
Accepted 27 February 2023
Available online 28 February 2023

Keywords:
Martensitic transformation
Magnetic shape memory alloys
Ni-Fe-Ga-Co Heusler alloys
Rapid solidification techniques

ABSTRACT

An almost single phase 14 M modulated martensite is obtained in melt spun ribbon of $Ni_{55}Fe_{17}Ga_{26}Co_2$ Heusler alloy. The effect of thermal treatments on the stability of the reverse martensitic transformation from 14 M modulated martensite to austenite phase in this system has been investigated by both non-isothermal and isothermal treatments. Heating above martensitic transformation promotes a continuous reduction of the martensitic transformation temperature, which stabilizes the austenite phase at room temperature and induces the precipitation of the gamma phase. However, thermal treatments at temperatures between the austenite start and finish temperatures induce the decoupling of the austenite formation in a subsequent heating. The two successive reverse martensitic transformations could be ascribed to the untransformed martensite in the previous interrupted heating and to the new martensite formed during cooling.

1. Introduction

Shape memory effect is based on the martensitic transformation that takes place in some materials as a first order structural transition, which involves a simultaneous, cooperative movement of atoms at a distance less than one interatomic distance and without long-range migrations of atoms. In the case of ferromagnetic systems, this kind of transformation overlaps with the occurrence of ferromagnetism, and thus is sensitive to magnetic field, as it was originally observed in 1996 by Ullako in Ni-Fe alloys [1]. The coupling between structural and magnetic transitions leads to unequivocal superiority over other smart materials in terms of possible applications, due to these first order phase transformations implies significant magnetization changes and improvements of related properties. This effect has been extensively analyzed in Ni-based Heusler alloys [2–4], being the most studied series the Ni-Mn-Ga [3]. However, the poor mechanical properties of the Ni-Mn-Ga Heusler alloys has induced the search for alternative compositions, leading the focus in Ni-Fe-Ga alloys with improved ductility and toughness by the introduction of small precipitates of gamma (disordered fcc) phase [5].

In Ni-Fe-Ga alloys, martensitic transformation (MT) occurs on cooling from an austenite, with disordered B2 or ordered $L2_1$ structure, to either a modulated or non-modulated martensite structure, which depends on composition, thermal history and preparation method [6–8]. Although a small amount of the secondary gamma phase is beneficial for the mechanical properties of the system, a high quantity inhibits the shape memory properties. In this sense, rapid quenching preparation techniques avoid the precipitation of the secondary phase in alloys with low Ga content (< 27 at%). Thus, the aim of producing these compositions by ultra-rapid quenching techniques such as melt-spinning is to obtain single phase systems without γ precipitates, which fraction can be finely tuned by subsequent annealing procedures to optimize the mechanical and magnetic properties. Therefore, the melt-spun samples, although crystalline, exhibit high atomic disorder and large strains, as typical characteristics induced by the preparation route and, thus, are in a metastable state. This metastability can lead to both reversible and irreversible transformations. Reversible effects are observed when the treatment temperature is not surpassed. Once temperature exceeds that of the thermal treatment, irreversible effects (shift of the martensitic transformation) appear. In fact, it has been shown that martensitic transformation in melt-spun $Ni_{55}Fe_{19}Ga_{26}$ Heusler alloy is very sensitive to thermal treatments above the martensitic transformation. However, this dependence of

* Corresponding author.
E-mail address: afmanchon@us.es (A.F. Manchón-Gordón).

https://doi.org/10.1016/j.jallcom.2023.169484

the martensitic transformation with thermal treatments has not been observed in samples of the same composition prepared by arc-melting, in which the parameters of the transformation (martensite temperature and enthalpy) are almost constant [8].

In order to shed some light about the reversibility and the metastable character of the samples produced by rapid quenching, the present work provides a detailed analysis of the thermal dependence of the martensitic transformation in a $Ni_{55}Fe_{17}Ga_{26}Co_2$ Heusler alloy prepared by melt-spinning and submitted to different isothermal and non-isothermal treatments. The reason for selecting this composition is two-fold: i) Ni-Fe-Ga systems with low Ga content cannot be produced as-single phase by conventional route and ii) the incorporation of Co facilitates the formation of the gamma phase in the subsequent heating treatments [9]. Moreover, it has been shown that the addition of Co can easily tune the martensitic transformation in Ni-Fe-Ga alloys depending on the element which Co is partially substituted for [10,11].

The results presented in this work are complementary to previous studies of the authors on Co-free composition for which different aspects of Ni-Fe-Ga ribbon Heusler alloy have been addressed: i) the effect of pressure on the martensitic transformation [7], ii) the differences between the ribbon and bulk structure [8] and iii) the thermal arrest of the reverse martensitic transformation [12].

2. Experimental

A $Ni_{55}Fe_{17}Ga_{26}Co_2$ Heusler alloy was synthesized from high purity elements in an induction furnace. The obtained ingots were melted several times in order to ensure homogeneity of the sample. Subsequently, ingots were induction melted in a quartz tube under Ar atmosphere and ejected onto a rotating copper wheel with a surface velocity of 20 m/s. The thickness and width of the ribbon are about 25 μm and 5 mm, respectively.

The chemical composition of the sample was determined by X-ray fluorescence (XRF) using an EAGLE III instrument with an anticatode of Rh. For the identification of present phases and the analysis of lattice parameters, X-ray diffraction measurements were carried out in a Bruker D8 Advance A25 diffractometer (Cu-Kα, λ=1.5406 Å). Mössbauer spectroscopy measurements were performed in transmission geometry using a ^{57}Co(Rh) source. Values of hyperfine parameters were obtained by fitting the obtained spectra with NORMOS program [13]. Macroscopic magnetic characterization of the alloy was performed in a vibrating sample magnetometer (standard option of a Quantum Design Physical Properties Measurement System, PPMS) applying different magnetic fields and a heating/cooling rate of ± 1 K/min.

The martensitic transformation was characterized under Ar flow by differential scanning calorimetry, DSC, (Perkin-Elmer DSC7 equipped with a cooling system) by isothermal and non-isothermal treatments. Measured temperature was corrected at different heating/cooling rates using the melting temperature of In standard (429.75 K) with an error below 0.5 K. The mass of the analyzed pieces of the ribbons was ~20 mg, close to that of the In standard. In order to observe the melting process of the samples, a TA Instruments SDT Q600 calorimeter was used at 20 K/min up to 1673 K.

3. Results and discussion

3.1. Microstructural and magnetic characterization

Table 1 collects the obtained results on composition by XRF chemical composition from both the free and the wheel side of the as-spun ribbon. Small composition differences between both sides of the ribbon and the nominal ones can be observed, probably due to preferential oxidation of the free side. On the other hand, elemental mapping of the sample shows a homogeneous distribution of the elements in the micrometer scale. Electron valence concentration per atom, e/a, also included in Table 1, was calculated from the sum of external d and s electrons for Ni (10), Fe (8) and Co (9), and s and p for Ga (3).

Table 1
Chemical composition estimated by XRF and electrons per atom (e/a) on both sides of $Ni_{55}Fe_{17}Ga_{26}Co_2$ melt-spun ribbon. Errors are taken as the standard deviation.

	at% Ni	at% Fe	at% Ga	at% Co	e/a
Nominal	55	17	26	2	7.82
wheel side	54.5±0.1	17.5±0.2	26.0±0.2	2.0±0.4	7.81±0.07
free side	53.9±0.1	17.5± 0.2	26.6±0.2	2.0±0.4	7.77±0.07

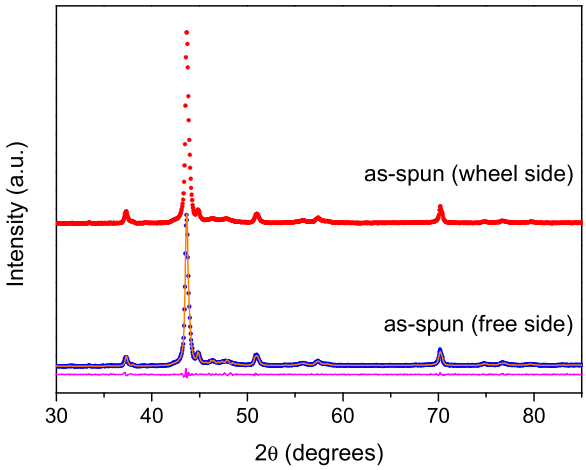

Fig. 1. XRD patterns of $Ni_{55}Fe_{17}Ga_{26}Co_2$ as-spun ribbon for the wheel (upper) and the free (bottom) sides, respectively. For the free side, Le Bail fitting for XRD pattern of the as-spun ribbon with P2/m space group. Symbols and solid lines correspond to observed and calculated patterns, respectively. The difference plot is shown at the bottom.

Fig. 1 shows the X-ray patterns obtained at room temperature from both the wheel and the free surfaces of the as-spun ribbon. Very similar patterns are obtained indicating that the small compositional differences detected by XRF do not affect the crystalline structure. The XRD patterns were assigned to a 14 M modulated martensite structure (space group $P2/m$) by Lebail refinement. The obtained lattice parameters (a=4.309(2) Å, b= 30.309(2) Å and c= 5.614(2) Å, GOF= 1.3), with b~7a, show a seven fold increase in the unit cell length along b axis, in agreement with the expected periodicity of the modulation. No other phases were needed to fully fit the XRD pattern of the as-spun sample, neither oxides nor γ-phase. Similar results have been reported for Co-free Ni-Fe-Ga alloys prepared by melt-spinning technique [8].

Fig. 2 shows the heat flow recorded in a SDT Q600 calorimeter at 20 K/min for a melt-spun ribbon. As it can be observed in the high temperature range (layer b), melting process of the as-spun ribbon (black curve) occurs almost in a single event that indicates the close to eutectic character of the transformation. However, on cooling (red curve), the solidification process occurs in several steps (at least four events are detected). The observed differences between both processes may be understood as the solid formed during cooling at 20 K/min strongly differs from the solid developed previously to melting from heating the metastable as-spun ribbon. At lower temperatures (layer a), despite the baseline effects, reverse martensitic transformation is clearly appreciated on heating as an endothermic process at ~600 K (red arrow in Fig. 2) and further weaker transformations are detected above this temperature (e.g. exothermic event at about 750 K marked with a green arrow in Fig. 2).

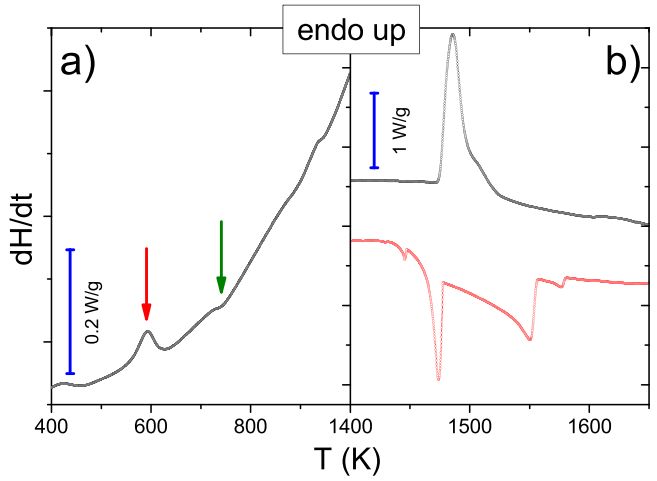

Fig. 2. Heat flow registered in a SDT Q600 calorimeter at 20 K/min of $Ni_{55}Fe_{17}Ga_{26}Co_2$ as-spun ribbon. a) Red arrow indicates reversible endothermic reverse martensitic process. Green arrow indicates irreversible exothermic process ascribed to the formation of γ phase. b) Black curve is the continuation of scan in a) and red curve corresponds to cooling at 20 K/min (only shown for the solidification process). Notice temperature and heat flow scales are different for the melting range.

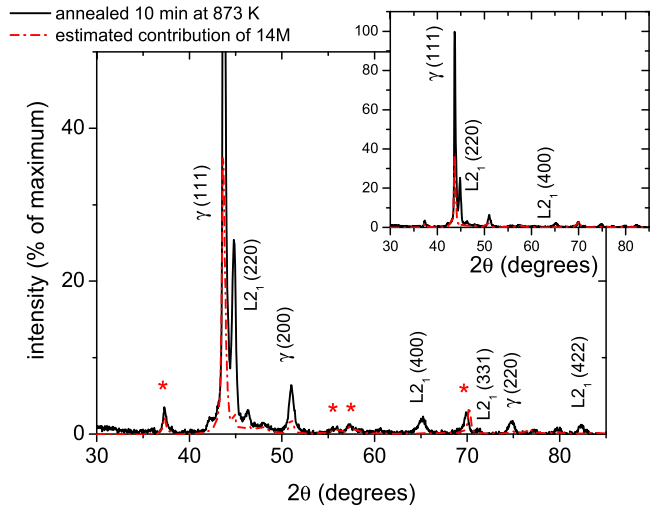

Fig. 3. XRD pattern for sample annealed 10 min at 873 K (black solid line) along with the estimated contribution of martensite phase to this pattern (red area). $L2_1$ (Cu_2MnAl type; space group $Fm\bar{3}m$, 225) and gamma (space group $Pm\bar{3}m$, 221) phases are indexed. Asterisks correspond to non-overlapped maxima of 14 M remanent phase. Inset shows the complete intensity range to appreciate the effect of the martensite contribution.

In fact, after annealing the ribbon at 873 K for 10 min, microstructural changes occur; gamma phase precipitates and austenite phase is stabilized at room temperature, as it is shown in Fig. 3. Distinction between $L2_1$ and B2 structures could be detected by the presence of (111), (311) and (331) maxima as demonstrated for NiMnInSi Heusler alloy [14]. However, in the studied case, the $L2_1$ or B2 structure for the austenite phase cannot be distinguished in the present composition, by experiments performed, due to the similarity between the different constituents. However, some remanent martensite phase is still detected and the similarities between the interplanar spacing of all the three phases make not straightforward the identification of the different maxima due to overlapping between them. In situ XRD experiments performed in a temperature controlled chamber only show the 14 M martensite phase below the transition and the austenite one above it without any evidence of the presence of intermartensitic transformations (XRD patterns not shown). In order to clarify this point, we proceeded as follows. Firstly; intensity ratios of 14 M phase were considered unaffected by annealing. Once this is assumed, we compared the intensities of those non-overlapped 14 M maxima detected in the annealed sample (marked with asterisks in Fig. 3). Finally, we rescaled and averaged the experimental patterns from the free and wheel sides of the as-spun sample (red dash-dotted line in Fig. 3). This allows us to confirm the presence of $L2_1$ and gamma phases in the sample annealed at 873 K.

From the angular position, 2θ, of the different diffraction maxima (h k l) of the $L2_1$ and gamma cubic phases, lattice parameters can be calculated from the linear fitting of $\ln(\sin^2(\theta))$ vs $\ln(h^2 + k^2 + l^2)$ derived from the Bragg law. This analysis leads to 5.68(3) Å and 3.577(14) Å, for the $L2_1$ and gamma phases, respectively. The composition of the remanent martensite phase may also coherently change as it can be inferred from the shift of the diffraction maximum at 2θ~70°. In the case of $L2_1$ phase, the low lattice parameter implies a number of electrons per atom $e/a > 8.1$ [15], which is clearly higher than those corresponding to the nominal composition, 7.82 (see Table 1). This indicates that the austenite phase must be enriched in Ni and depleted in Fe with respect to the average nominal composition. This could be explained as follows: neglecting Ga content in gamma phase, from e/a parameter, Ni content in γ-$Fe_{100-x}Ni_x$ could be estimated from the lattice parameter as 56±10 at % [16], which implies a Fe/Ni concentration ratio for gamma phase of 0.79, which is much larger than the nominal value, 0.35 (even considering Fe+Co content). Therefore, after annealing at 873 K, precipitation of gamma phase is observed, with a preferential partitioning of Fe to the gamma phase and, consequently, austenite $L2_1$ phase is enriched in Ni.

Fig. 4 (left) shows the room temperature Mössbauer spectra of the as-spun ribbon and of the ribbon annealed 10 min at 873 K. These spectra have been fitted using two distributions of hyperfine fields, B_{hf}: a high field distribution from 5 to 30 T (blue line in Fig. 4) to describe the ferromagnetic (FM) contributions, and a second distribution from 0 to 7.5 T (red line in Fig. 4) to describe the paramagnetic (PM) contributions. The use of this artificial B_{hf} contribution to represent PM sites avoids difficulties in the convergence of the fitting of the spectra with respect to the use of a more realistic fitting, which would use a quadrupolar distribution to describe the PM contributions [17]. Therefore, only fraction area would have physical meaning for this second distribution. The corresponding probability distributions of B_{hf} can be observed in Fig. 4 (right). According to the XRD measurements, the as-spun ribbon only exhibits a unique phase: the modulated 14 M martensite phase. However, Fe environments are complex and not well defined as the necessity to use distributions suggests. Moreover, the presence of PM contributions is also clear. This could be due to the presence of a distribution of Curie temperatures, typically found in systems obtained by rapid quenching such as melt-spinning [18]. However, the small contributions above 20 T could correspond to ferromagnetic impurity phases, possibly gamma phase, as Mössbauer spectroscopy is more sensitive than XRD to detect such contributions [19]. Annealing 10 min at 873 K led to an increase of the contributions between 12 and 15 T, compensated by a reduction of the PM contributions. Despite the clear detection of gamma phase by XRD, contributions at high B_{hf} values remain small. This indicates that the gamma phase formed during annealing should correspond to B_{hf} contributions between 15 and 20 T (contributions that clearly increased after annealing), and thus with a much lower Curie temperature than that corresponding to the FM impurities already observed in the as-spun sample (B_{hf} >20 T).

Magnetization measurements may help in the understanding of Mössbauer results. Fig. 5 shows the specific magnetization, at an applied field of 100 Oe (0.01 T), as a function of the temperature, $\sigma(T)$, obtained in a PPMS device for the as-spun sample and the

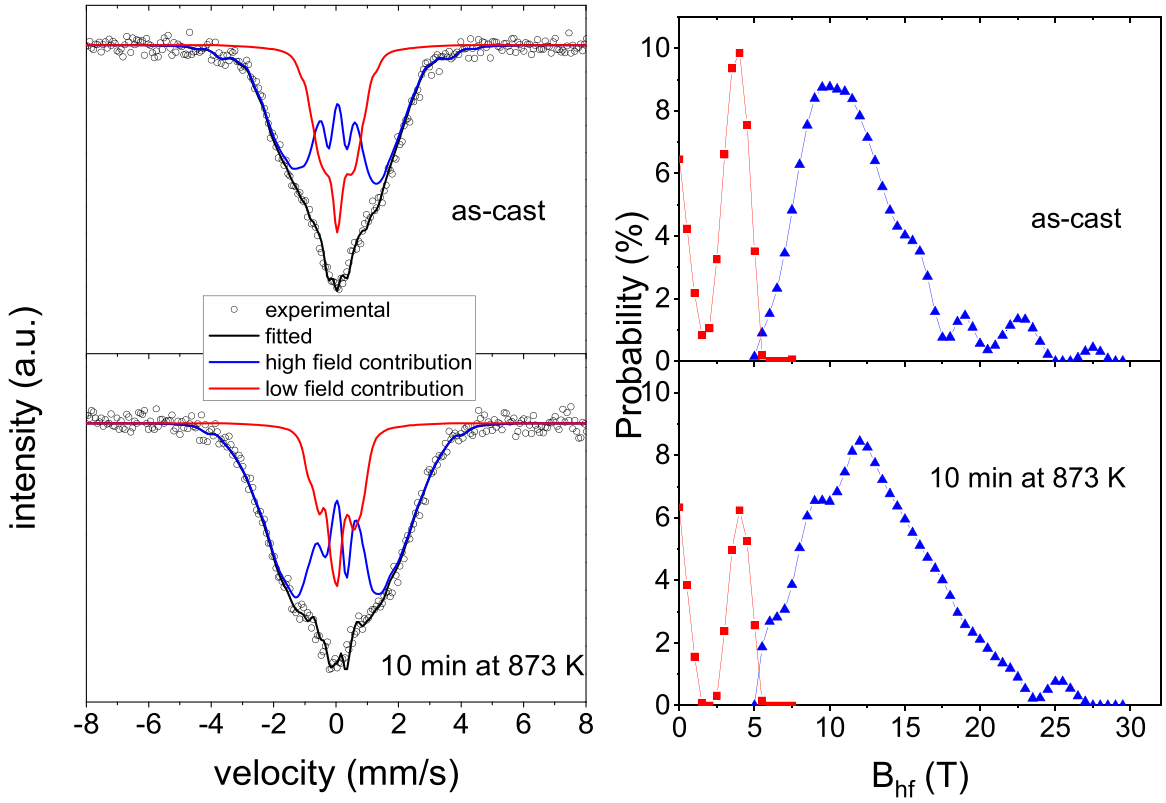

Fig. 4. Left: Room temperature Mössbauer spectra (symbols) and model fitting (lines) of $Ni_{55}Fe_{17}Ga_{26}Co_2$ as-spun and annealed 10 min at 873 K ribbons. Right: corresponding probability distributions of hyperfine fields (square and triangles correspond to low and high field contributions, respectively).

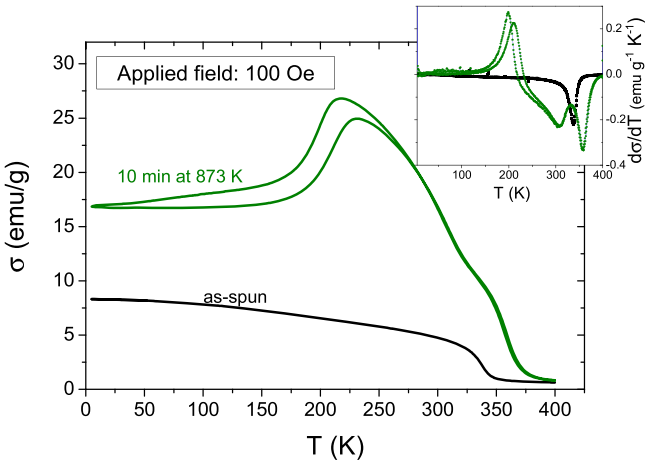

Fig. 5. Temperature dependence of the specific magnetization of $Ni_{55}Fe_{17}Ga_{26}Co_2$ as-spun ribbon and sample annealed 10 min at 873 K. Inset shows the corresponding derivative curves of σ(T).

sample annealed 10 min at 873 K (measurement corresponds to cooling from 400 K). In the case of the as-spun sample, a single Curie event is observed in the studied range. Following the XRD results (Fig. 1), this transition corresponds to the magnetic transformation of the 14 M martensite modulated structure (T_C^{14M}=338 K). This value is slightly higher than those obtained for Co-free Ni-Fe-Ga Heusler alloys prepared by melt-spinning (T_C^{14M}=320 K) [8]. Moreover, a remanent magnetization is observed above this transition up to the limit of the equipment. When this remanent magnetization (σ∼0.6 emu/g) is ascribed to the presence of ferromagnetic γ-phase, a fraction of ∼0.5% can be inferred (assuming an approximate composition for the γ-phase of $Fe_{25}Ni_{75}$ with T_C^{γ}∼875 K and σ∼100 mu/g [16]). This small fraction, on the one hand, can explain why it is not detected from XRD and, on the other hand, it could be ascribed to the hyperfine field contributions beyond 20 T observed from Mössbauer spectroscopy and corresponding to FM impurities (∼3% of Fe atoms). In the case of the annealed ribbon, this magnetization value at 400 K is similar to that obtained in the case of the as-spun ribbon (in agreement with similar high B_{hf} contribution found for both samples by Mössbauer study) and should be ascribed to gamma phase crystallites already formed in the melt-spun ribbon.

Unlike as-spun sample, the thermomagnetic curves of the sample annealed up to 873 K reveal several transitions. Following the XRD and DSC results (see next section), these transitions can be identified. In fact, during cooling, the sample undergoes a first magnetic transition from PM gamma to FM gamma phase at the Curie temperature of this phase (T_C^{γ}=359 K). This gamma phase would correspond to the clearly detected one from XRD and its Curie temperature should correspond to values below 30 at% of Ni (highly enriched in Fe), in rough agreement with XRD results that pointed to ∼40 at% of Ni from the lattice parameter of the gamma phase. It is worth mentioning that Ga content in gamma phase has been neglected in these estimations and its effect should be stronger in the Curie temperature than in the lattice parameter. At 307 K, a PM to FM transition ascribed to the austenite phase can be observed ($T_C^{L2_1}$=307 K). Therefore, the Curie temperature of the austenite phase is lower than the Curie temperature corresponding to the martensite phase in as-spun sample. However, the formation of gamma phase and the asymmetric partitioning of Fe and Ni to austenite and gamma phases must affect the composition. Finally, the transformation from FM austenite to FM martensite occurs at T_M∼200 K. The obtained values are similar to those collected by Tolea et al. in thermally treated ribbons of Ni-Fe-Ga-Co system [20]. The observed MT in this sample is a broad transition, which extends from 210 K to below 150 K, and it is magnetically evidenced only at low applied

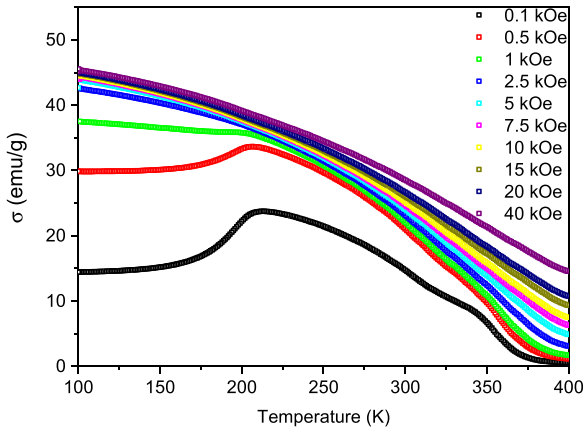

Fig. 6. Temperature dependence of magnetization (on cooling) at different magnetic applied fields for the ribbon annealed 10 min at 873 K.

magnetic fields. This is because, although the magnetic anisotropy of the martensite phase is higher than that of the cubic austenite phase, saturation magnetization values must be similar. Therefore, the increase of the magnetic field avoids the observation of the MT due to the similar saturation magnetization (and atomic magnetic moment) of both phases, as it is shown in Fig. 6.

3.2. Non-isothermal treatments

The effect of thermal treatment on the MT of the studied ribbons was studied by in-situ DSC experiments. Fig. 7a shows the virgin curve (i.e. the first heating DSC scan for the as-spun ribbon) up to 673 K at 20 K/min along with the following two cooling and heating cycles up to the same temperature using the same heating rate (transitory signals occurring at the changes of heating rate are removed for clarity). DSC curves present exothermic (on cooling) and endothermic (on heating) peaks related to the forward and reverse MT, respectively. Moreover, the calorimetric scans reveal that the peak temperature of the reverse martensitic transformation strongly decreases after the first heating, but it keeps invariable in the subsequent cycles when the maximum temperature achieved is preserved. In the following, samples to be studied were initially heated to 673 K at 20 K/min to minimize the effects of the virgin curve. This protocol will be named as the relaxation protocol and has been applied previously to study the stability and kinetics of the MT in Co free Ni-Fe-Ga alloys [8,21].

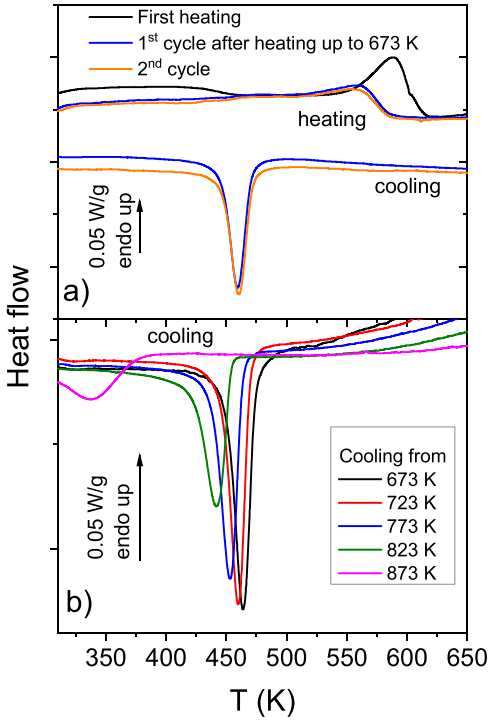

Fig. 7. Consecutive DSC scans showing a) the effect of thermal cycling on the martensitic transformation when the sample is heated up to the same maximum temperature (673 K) and b) the evolution of the martensitic temperature when samples are cooled from progressively higher temperatures above the martensitic transformation.

To evaluate the stability of the MT in the studied ribbons, different thermal cycles were carried out up to progressively higher temperatures each time. Fig. 7b shows the cooling DSC scans of the ribbons after heating up to the indicated temperatures above MT. For clarity, only the cooling branch of the cycles, corresponding to the direct (austenite to martensite phases) martensitic transformation, are represented. As maximum heating temperature increases, there is a progressive decrease of the peak temperature of the austenite to martensite transformation (1.5 K decrease per each 10 K increase in the maximum temperature of the previous heating). However, this decrease is enhanced when heating exceeds the temperature of formation of gamma phase and a decrease > 100 K in peak temperature of the transformation is observed when maximum heating temperature changes from 823 to 873 K.

Fig. 8 shows the evolution of the martensite start temperature, M_{start}, determined from DSC curves given in Fig. 7b and the transformation enthalpy in the direct martensitic transformation, ΔH, as a function of the upper limit temperature reached in each cycle for relaxed samples. We can distinguish between the behavior of samples heated below and above the relaxation temperature (673 K). The M_{start} remains almost constant when cycles are performed at temperatures lower than 673 K (the temperature at which the virgin ribbon was previously heated). However, a clear increase of ΔH can be observed in this range of temperatures, which is just an indication of the fraction of austenite phase formed during transformation. This value saturates once all the austenite phase is formed, for samples heated above 575 K (see the heating curves in Fig. 7a). For samples heated above 673 K, both parameters, M_{start} and ΔH, continuously decreases with increasing the upper limit temperature. The obtained results suggest a structural modification of the ribbon during the thermal treatments, in agreement with the previously reported results for ribbons of Ni-Fe-Ga [8] and Ni-Fe-Ga-Co Heusler alloys [20]. Reduction of ΔH can be interpreted as a progressive

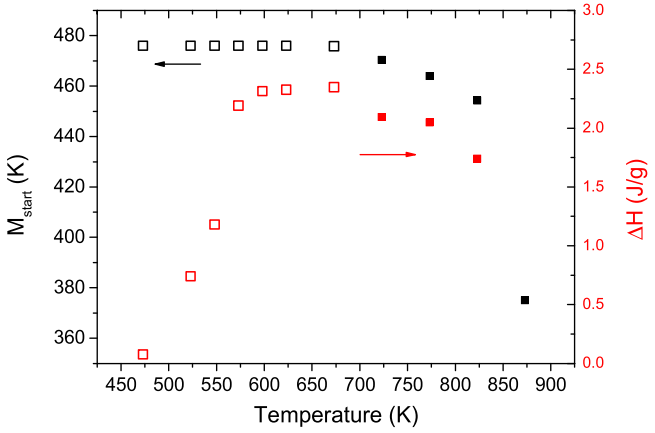

Fig. 8. Martensitic transformation start temperature and heat of transformation as a function of the upper limit temperature reached in each cooling-heating cycle. Hollow symbols correspond to samples submitted to treatments at temperatures below 673 K (to avoid virgin effects). Solid symbols correspond to samples treated at temperatures above 673 K and thus implying possible structural evolution.

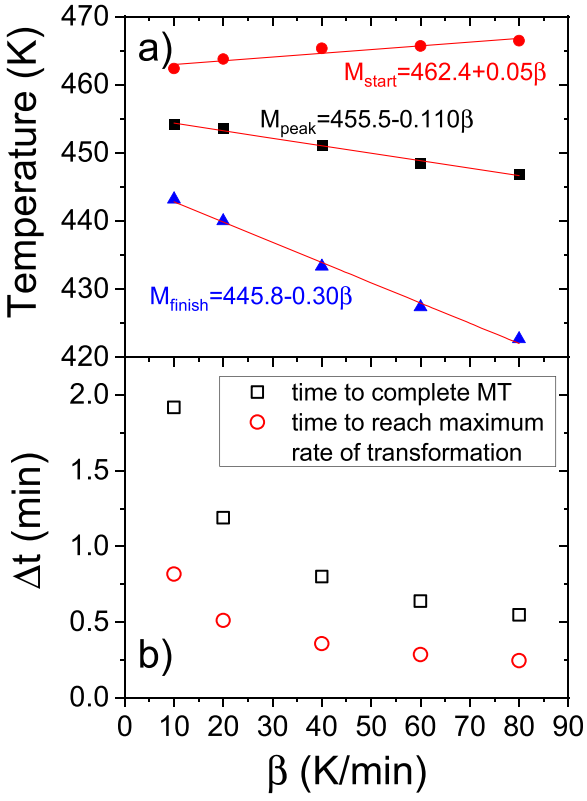

Fig. 9. a) Characteristic temperatures of the martensitic transformation. Lines correspond to linear fittings with the fitting parameters indicated. b) Time required to complete the transformation and time required to reach the maximum rate of transformation as a function of the cooling rate.

precipitation of γ phase, which should lead to changes in the composition of the remanent austenite to be transformed to martensite and could explain the shift to lower temperatures of MT (in fact, an enrichment in Ga in $Ni_{55}Fe_{17.5}Ga_x$ from x = 26.5–27.5% led to a decrease of more than 50 K in M_{start} [22]).

Calorimetric measurements with the cooling rate changing from β = −5 to − 80 K/min were also performed on the samples heated up to 673 K (to avoid virgin effects) to identify the dependence of MT on β. Fig. 9a displays the relationship between the values of the martensite start, M_{start}, finish, M_{finish}, and peak, M_{peak}, temperatures and the cooling rate. The value of M_{start} remains almost constant, indicating that the onset of the transformation is athermal and not thermally activated. However, a shift to lower temperatures as cooling rate increases can be observed for both M_{peak} and M_{finish}. Fig. 9b shows the time interval required to complete the MT (calculated as $\Delta t = \frac{M_{finish} - M_{start}}{\beta}$) as a function of β. The abrupt rise as $\beta \rightarrow$ 0 K/min points to the transformation could not be completed in isothermal transformation. The linear correlation between the different characteristic temperatures and β allows us to estimate the limit value of $M_{finish} - M_{start}$=16.6 K for $\beta \rightarrow$ 0 K/min, which is higher than those obtained for Co-free Ni-Fe-Ga Heusler alloys with lower transition temperatures [12].

3.3. Isothermal treatments

Relaxed samples were submitted to two different isothermal treatments: below austenite finish temperature and above the relaxation temperature, 673 K. The former experiments are reversible and the sample can be recovered once the relaxation protocol (heating at 20 K/min up to 673 K) is repeated. The latter experiments lead to irreversible microstructural evolution of the samples (mainly precipitation of γ-phase).

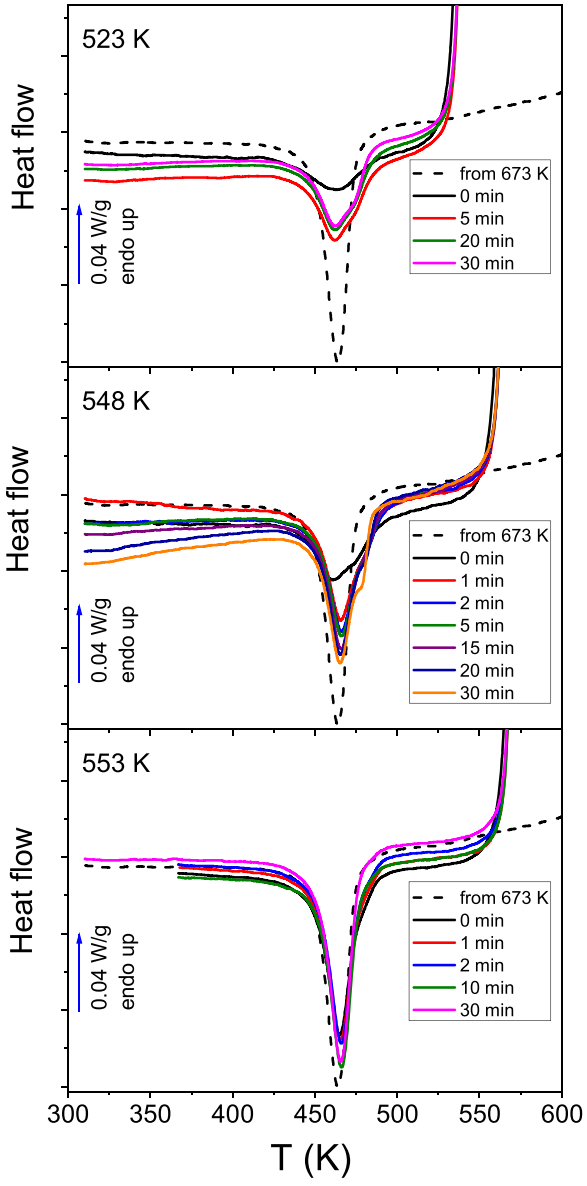

Fig. 10. Cooling DSC scans recorded at 20 K/min for samples isothermally treated during the indicated dwelling times at the indicated temperatures. The dashed curve corresponds to the reference sample that was relaxed by heating up to 673 K at 20 K/min to avoid virgin curve effects.

In order to determine the effect of the former, reversible, isothermal treatments on MT, the following DSC experiments were carried out: Firstly, samples previously heated up to 673 K (to avoid virgin effects) were heated at 20 K/min up to a temperature between austenite start, A_{start}, and finish, A_{finish}, temperatures. Afterwards, at this temperature, the reverse martensitic transformation was interrupted by means of an isothermal treatment (from 0 to 30 min) followed by cooling to room temperature at 20 K/min. The cooling processes after the isothermal treatments are depicted in Fig. 10, showing the partial direct martensitic transformation (in agreement with interrupted austenitic transformation) that occurs after the corresponding isothermal treatment. From this figure, it is evidenced the enhancement of the exothermic peaks upon cooling with the increase of the dwelling time for all the analyzed temperatures, corresponding to a further progress of the austenite development during the isothermal dwelling times. This is a characteristic of isothermal transformations (i.e. thermally activated processes). In

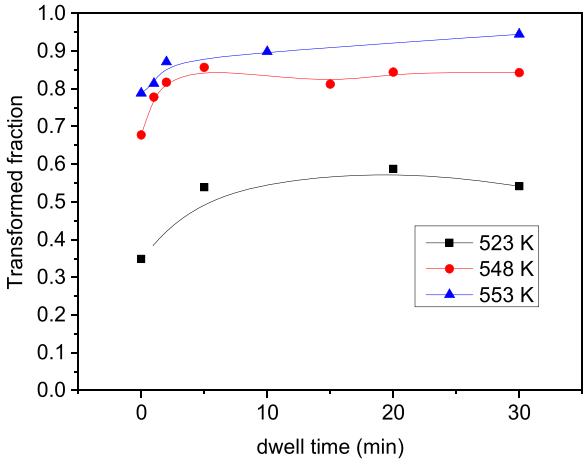

Fig. 11. Transformed fraction obtained by isothermal treatments as a function of dwell time at the indicated temperatures. Lines are just guide for the eye.

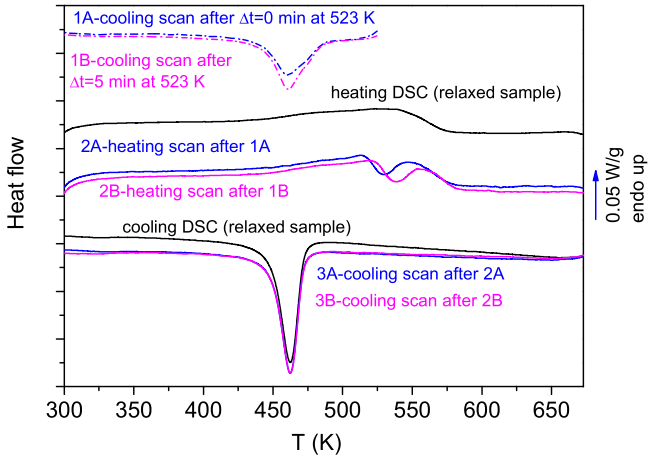

Fig. 12. DSC curves, at 20 K/min, corresponding to cooling down to room temperature a relaxed sample heated up to 523 K and submitted to 0 and 5 min isotherm (1 A and 1B, respectively). Subsequent heating DSC curves to 673 K (2 A and 2B curves, respectively) and, finally, cooling DSC curves after these treatments (3 A and 3B respectively). Heating and cooling curves of the relaxed sample are shown for comparison. The DSC record becomes reversible after heating to 673 K (compare 3 A and 3B to that of the relaxed sample).

fact, on cooling, both shape and magnitude of MT changes with dwelling time.

The enthalpy change of the MT measured on cooling experiments can be used to estimate the austenite phase fraction obtained during the isothermal process taking as 100% that of the relaxed ribbon (dotted line). The results of this analysis are shown in Fig. 11. As it can be observed, a clear increase of the transformed fraction with the increase of dwelling time is achieved, which is characteristic of isothermal processes. However, the increase of the transformed fraction occurs for the shorter dwelling times, while saturation below 100% is rapidly obtained and no important differences can be observed at longer dwelling times. This result indicates that the isothermal character of the transformation is limited and isothermal and athermal character of the transformation coexist. Different factors can contribute to the observed time-dependence of the MT in the studied samples, including relaxation processes [23,24] and the development of strain nanodomains [25]. In fact, partial isothermal nature of the MT was found in non-stoichiometric Ti-Ni alloys, but not observed in the equiatomic TiNi alloy [25]. In the studied alloy, the accumulation of the elastic energy due to the non-stoichiometric composition and the typical disorder of the alloys prepared by rapid quenching [26] could be a reasonable argument to understand partial development of the MT by isothermal treatments.

The influence of interrupting the heating during the reverse martensite transformation has been analyzed through the corresponding subsequent DSC scan in which the MT is completed (i.e. scan up to 673 K that follows the cooling scans shown in Fig. 10). Despite the sample was cooled to room temperature, well below M_{finish}, the effects of the isothermal treatments during the austenite formation are not erased but heating curves present memory of the isothermal treatments. Fig. 12 shows the cooling curves after interrupted austenite formation at 523 K (1 A and 1B curves), as well as the subsequent heating curves (2 A and 2B curves). The heating DSC curve corresponding to the relaxed sample is also shown for comparison. All those heating curves were performed at 20 K/min up to 673 K (relaxation protocol) and the corresponding subsequent cooling curves are also shown to evidence the reversibility of this process (3 A and 3B curves).

Remarkable effects on the reversal MT can be observed. The DSC heating curves after 0 and 5 min at 523 K thermal treatment (2 A and 2B in Fig. 12) show two partially decoupled endothermic peaks instead of the single one observed in the virgin curve corresponding to the relaxed sample. On the one hand, this effect can be associated with the development of intermartensitic transformations between modulated and non-modulated martensite phases which has been previously observed in other Ni-based shape memory alloys [6,27,28]. However, the deconvolution of the martensitic transformation only occurs during heating process and remains without changes in the case of the cooling process. Moreover, in situ XRD experiments performed in a temperature controlled chamber did not show, in the present case, the presence of intermartensitic transformation but just low temperature 14 M martensite and high temperature austenite phase (XRD patterns not shown). On the other hand, this decoupling phenomenon of the reversal MT has been previously reported for $Ni_{45}Ti_{51.8}Fe_{3.2}$ shape memory alloy and attributed to the creation of local stress fields [29]. In any case, the coexistence of the two successive transformations broadens the phase transformation temperature span of the martensite to austenite phase. Thus, this effect could be interesting for caloric applications of the studied material [30]. It is worth mentioning that any effect of the isothermal treatments can be erased once the sample is heated up again to the relaxation temperature, 673 K (see 3 A and 3B curves in Fig. 12). Therefore, under these circumstances, the processes are completely reversible. The obtained results are similar to those reported in studies that analyze the effect of interruption of the martensitic transformation, finding that non-complete cycles can significantly affect the transformation behavior in shape memory alloys in the subsequent complete transformation cycle [31–33]. This phenomenon, which has been called thermal arrest memory effect, has been also reported in Ni-Mn-Ga Heusler alloys [34] and recently in Ni-Fe-Ga polycrystalline ribbons [12], but it has not been previously reported in Ni-Fe-Ga-Co alloys. Moreover, it is typically analyzed only as a function of temperature, while here, the effect of thermal arrest dwelling time on the MT has been also investigated. In this sense, the deconvolution of MT clearly depends on dwelling time, leading to an increase in the broadening of the transformation as it increases. This effect can be related to an increase in domain walls regions between the different martensite variants as the dwelling time increases [12].

On the other hand, it is clearly observed that the enthalpy registered in MT process increases as isothermal time increases (as it was already shown in Fig. 8). Moreover, the effect of interrupting the reversal MT is to shift part of the transformation to lower temperatures. This shifted fraction of the transformation increases as dwell time increases, while there is a remaining fraction of the process that seems to be unaffected. That shifted fraction of the process can be identified with the austenite phase that was

developed during the interrupted transformation. These regions, when cooling down in MT, transform to a martensite phase that is less stable than the original one, probably due to extra stresses developed at the boundary between this new martensite and the untransformed one during the interrupted reversal MT.

4. Conclusions

$Ni_{55}Fe_{17}Ga_{26}Co_2$ Heusler alloy, developed by melt-spinning, exhibits an almost single martensite phase with a 14 M modulated structure at room temperature. Although this is the unique phase detected by X-ray diffraction, Mössbauer spectroscopy and magnetometry results indicate the presence of a minority ferromagnetic gamma phase. The martensite phase reversibly transforms to austenite cubic phase at about 480 K. This reversible character remains for treatments below 673 K. However, thermal treatments above this temperature lead to the precipitation of a Fe enriched gamma phase which leads to the shift of the martensitic transformation to lower temperatures as the austenite phase becomes enriched in Ni. The metastable character of the system remains even up to the melting process which occurs in a close to eutectic process.

Athermal character of the martensite transformation can be observed in the onset of the transformation as it does not depend on cooling rate. However, the time required for the transformation decreases as cooling rate increases indicating that the kinetics of the process accelerates up as temperature increases. Moreover, isothermal treatments performed in the temperature range of the reversal martensite transformation show a certain isothermal character of the transformation as the fraction of austenite phase increases with the increase of the dwell time.

Interruption of isothermal treatments during reversal martensitic transformation leads to a decoupling of the formation of the austenite phase during the subsequent heating process due to the shift to lower temperatures of a fraction of the transformation related to the previously formed austenite during the isothermal treatment.

Credit authorship contribution statement

A.F. Manchón-Gordón: Conceptualization, Experiments, Formal analysis, Resources, Writing – original draft, Resources, **A. Vidal-Crespo:** Experiments, Formal analysis, Writing – review & editing, **J.S. Blázquez:** Conceptualization, Methodology, Supervision, Writing – original draft, Resources, **M. Kowalczyk**: Experiment, Supervision, Writing – review & editing, **J.J. Ipus**: Experiment, Supervision, Writing – review & editing, **T. Kulik**: Resources, Writing – review & editing, **C.F. Conde**: Resources, Methodology, Supervision, Writing – review & editing.

Data availability

Data will be made available on request.

Declaration of Competing Interest

The authors declare that they have no known competing financial interests or personal relationships that could have appeared to influence the work reported in this paper.

Acknowledgements

This work was supported by PAI of the Regional Governement of Andalucía and VII PPIT of University of Sevilla (financing DSC measurements at CITIUS) and by Junta de Andalucía-Consejería de Universidad, Investigación e Innovación (project ProyExcel_00360). A. Vidal-Crespo acknowledges a VPPI-US fellowship.

References

[1] K. Ullakko, Magnetically controlled shape memory alloys: a new class of actuator materials, J. Mater. Eng. Perform. 5 (3) (1996) 405–409.
[2] A. Planes, L. Mañosa, M. Acet, Magnetocaloric effect and its relation to shape-memory properties in ferromagnetic Heusler alloys, J. Phys.: Condens. Matter 21 (23) (2009) 233201.
[3] T. Graf, C. Felser, S.S.P. Parkin, Simple rules for the understanding of Heusler compounds, Prog. Solid State Chem. 39 (1) (2011) 1–50.
[4] T. Bachaga, J. Zhang, M. Khitouni, J.J. Sunol, NiMn-based Heusler magnetic shape memory alloys: a review, Int. J. Adv. Manuf. Technol. 103 (5) (2019) 2761–2772.
[5] J. Pons, E. Cesari, C. Seguí, F. Masdeu, R. Santamarta, Ferromagnetic shape memory alloys: alternatives to Ni–Mn–Ga, Mater. Sci. Eng.: A 481 (2008) 57–65.
[6] R.F. Hamilton, H. Sehitoglu, C. Efstathiou, H.J. Maier, Inter-martensitic transitions in Ni–Fe–Ga single crystals, Acta Mater. 55 (14) (2007) 4867–4876.
[7] A.F. Manchón-Gordón, J.J. Ipus, M. Kowalczyk, A. Wójcik, J.S. Blázquez, C.F. Conde, W. Maziarz, P. Švec Sr, T. Kulik, A. Conde, Effect of pressure on the phase stability and magnetostructural transitions in nickel-rich NiFeGa ribbons, J. Alloy. Compd. 844 (2020) 156092.
[8] A.F. Manchón-Gordón, J.J. Ipus, M. Kowalczyk, J.S. Blázquez, C.F. Conde, P. Švec, T. Kulik, A. Conde, Comparative study of structural and magnetic properties of ribbon and bulk Ni55Fe19Ga26 Heusler alloy, J. Alloy. Compd. 889 (2021) 161819.
[9] Y. Imano, T. Omori, K. Oikawa, Y. Sutou, R. Kainuma, K. Ishida, Martensitic and magnetic transformations of Ni–Ga–Fe–Co ferromagnetic shape memory alloys, Mater. Sci. Eng.: A 438–440 (2006) 970–973.
[10] K. Oikawa, Y. Imano, V.A. Chernenko, F. Luo, T. Omori, Y. Sutou, R. Kainuma, T. Kanomata, K. Ishida, Influence of Co Addition on Martensitic and Magnetic Transitions in Ni-Fe-Ga β Based Shape Memory Alloys, Mater. Trans. 46 (3) (2005) 734–737.
[11] M. Sofronie, F. Tolea, V. Kuncser, M. Valeanu, Martensitic transformation and accompanying magnetic changes in Ni–Fe–Ga–Co alloys, J. Appl. Phys. 107 (11) (2010) 113905.
[12] A. Vidal-Crespo, A.F. Manchón-Gordón, J.S. Blázquez, J.J. Ipus, P. Svec, C.F. Conde, Thermal arrest analysis of the reverse martensitic transformation in a Ni55Fe19Ga26 Heusler alloy obtained by melt-spinning, J. Therm. Anal. Calorim. (2022).
[13] R.A. Brand, J. Lauer, D.M. Herlach, The evaluation of hyperfine field distributions in overlapping and asymmetric Mossbauer spectra: a study of the amorphous alloy Pd77.5-xCu6Si16.5Fex, J. Phys. F: Met. Phys. 13 (3) (1983) 675–683.
[14] R. Das, P. Saravanan, D. Arvindha Babu, A. Perumal, A. Srinivasan, Influence of solidification rate and heat treatment on magnetic refrigerant properties of melt spun Ni51Mn34In14Si1 ribbons, J. Magn. Magn. Mater. 344 (2013) 152–157.
[15] S. Chabungbam, P. Borgohain, S. Ghosh, N. Singh, M.B. Sahariah, Martensitic transformation and magnetism in Ni and Fe-rich compositions of Ni-Fe-Ga shape memory alloys, J. Alloy. Compd. 689 (2016) 199–207.
[16] B. Glaubitz, S. Buschhorn, F. Brüssing, R. Abrudan, H. Zabel, Development of magnetic moments in Fe1 −xNix-alloys, J. Phys.: Condens. Matter 23 (25) (2011) 254210.
[17] A.F. Manchón-Gordón, L.M. Moreno-Ramírez, J.J. Ipus, J.S. Blázquez, C.F. Conde, V. Franco, A. Conde, A procedure to obtain the parameters of Curie temperature distribution from thermomagnetic and magnetocaloric data, J. Non-Cryst. Solids 520 (2019) 119460.
[18] A.F. Manchón-Gordón, R. López-Martín, A. Vidal-Crespo, I.J. J. J.S. Blázquez, C.F. Conde, A. Conde, Distribution of transition temperatures in magnetic transformations sources effects procedures to extract information from experimental, Data, Metals (2020).
[19] A.F. Manchón-Gordón, J.J. Ipus, J.S. Blázquez, C.F. Conde, A. Conde, Evolution of Fe environments and phase composition during mechanical amorphization of Fe70Zr30 and Fe70Nb30 alloys, J. Non-Cryst. Solids 494 (2018) 78–85.
[20] F. Tolea, M. Sofronie, A.D. Crisan, M. Enculescu, V. Kuncser, M. Valeanu, Effect of thermal treatments on the structural and magnetic transitions in melt-spun Ni-Fe-Ga-(Co) ribbons, J. Alloy. Compd. 650 (2015) 664–670.
[21] A.F. Manchón-Gordón, R. López-Martín, J.J. Ipus, J.S. Blázquez, P. Svec, C.F. Conde, A. Conde, Kinetic analysis of the transformation from 14M Martensite to L21 Austenite in Ni-Fe-Ga Melt Spun Ribbons, Metals 11 (6) (2021) 849.
[22] H.X. Zheng, M.X. Xia, J. Liu, J.G. Li, Martensitic transformation of Ni–Fe–Ga magnetic shape memory alloys, J. Alloy. Compd. 385 (1) (2004) 144–147.
[23] D. Salas, E. Cesari, J. Van Humbeeck, S. Kustov, Isothermal B2–B19′ martensitic transformation in Ti-rich Ni–Ti shape memory alloy, Scr. Mater. 74 (2014) 64–67.
[24] S. Kustov, D. Salas, R. Santamarta, E. Cesari, J. Van, Humbeeck, Isothermal and athermal martensitic transformations in the B2–R–B19′ sequence in Ni–Ti shape memory alloys, Scr. Mater. 63 (12) (2010) 1240–1243.
[25] N. Resnina, S. Belyaev, A. Shelyakov, Isothermal B2→B19′ martensitic transformation in Ti40.7Hf9.5Ni44.8Cu5 shape memory alloy, Scr. Mater. 112 (2016) 106–108.
[26] H.-R. Zhang, G.-H. Wu, Atomic-size effect on the microstructural properties of Ni2FeGa, Acta Mater. 59 (3) (2011) 1249–1258.
[27] Z. Li, K. Xu, Y. Zhang, C. Tao, D. Zheng, C. Jing, Two successive magneto-structural transformations and their relation to enhanced magnetocaloric effect for Ni55.8Mn18.1Ga26.1 Heusler alloy, Sci. Rep. 5 (1) (2015) 15143.

[28] F. Hu, S. Wei, Y. Cao, Z. Li, X. He, K. Xu, Y. Zhang, Y. Kang, H. Yang, Q. Zhang, Magnetocaloric and barocaloric effects associated with two successive magnetostructural transformations in Ni55.5Mn17.8Ga26.7 alloy, J. Alloy. Compd. 818 (2020) 153356.
[29] Y.-q Zhang, S.-y Jiang, X.-m Zhu, Y.-n Zhao, Y.-l Liang, D. Sun, Influence of Fe addition on phase transformation behavior of NiTi shape memory alloy, Trans. Nonferrous Met. Soc. China 27 (7) (2017) 1580–1587.
[30] X. Zhang, H. Zhang, M. Qian, L. Geng, Enhanced magnetocaloric effect in Ni-Mn-Sn-Co alloys with two successive magnetostructural transformations, Sci. Rep. 8 (1) (2018) 8235.
[31] Z.G. Wang, X.T. Zu, Y.Q. Fu, L.M. Wang, Temperature memory effect in TiNi-based shape memory alloys, Thermochim. Acta 428 (1) (2005) 199–205.
[32] K. Madangopal, S. Banerjee, S. Lele, Thermal arrest memory effect, Acta Metall. Et. Mater. 42 (6) (1994) 1875–1885.
[33] G. Airoldi, A. Corsi, G. Riva, Step-wise martensite to austenite reversible transformation stimulated by temperature or stress: a comparison in NiTi alloys, Mater. Sci. Eng.: A 241 (1) (1998) 233–240.
[34] M.Z. Zhou, X. Zhang, X.L. Meng, W. Cai, L.C. Zhao, Temperature memory effect induced by incomplete transformation in Ni-Mn-Ga-based shape memory alloy, Mater. Today.: Proc. 2 (2015) S867–S870.